ADVANCED FUNCTIONAL MATERIALS
www.afm-journal.de

The Effects of Electronic Impurities and Electron–Hole Recombination Dynamics on Large-Grain Organic–Inorganic Perovskite Photovoltaic Efficiencies

*Jean-Christophe Blancon, Wanyi Nie, Amanda J. Neukirch, Gautam Gupta, Sergei Tretiak, Laurent Cognet, Aditya D. Mohite, and Jared J. Crochet**

Hybrid organic-inorganic perovskites have attracted considerable attention after promising developments in energy harvesting and other optoelectronic applications. However, further optimization will require a deeper understanding of the intrinsic photophysics of materials with relevant structural characteristics. Here, the dynamics of photoexcited charge carriers in large-area grain organic-inorganic perovskite thin films is investigated *via* confocal time-resolved photoluminescence spectroscopy. It is found that the bimolecular recombination of free charges is the dominant decay mechanism at excitation densities relevant for photovoltaic applications. Bimolecular coefficients are found to be on the order of 10^{-9} cm^3 s^{-1}, comparable to typical direct-gap semiconductors, yet significantly smaller than theoretically expected. It is also demonstrated that there is no degradation in carrier transport in these thin films due to electronic impurities. Suppressed electron–hole recombination and transport that is not limited by deep level defects provide a microscopic model for the superior performance of large-area grain hybrid perovskites for photovoltaic applications.

1. Introduction

Direct band gap semiconductors with low defect densities, such as single crystalline GaAs, are the epitome of high efficiency optoelectronic devices. However these materials are obtained using expensive high temperature crystal growth techniques such as molecular beam epitaxy. Consequently, there has been a constant search over the last two decades for new materials that can be obtained using scalable solution based strategies. A major setback of solution-processed materials has been that most are plagued with polydispersity, lack of crystallinity, and unacceptable levels of electronic defects. Over the past few years solution-processed hybrid organic-inorganic perovskite semiconducting materials (mainly $CH_3NH_3PbI_3$ and $CH_3NH_3PbI_{3-x}Cl_x$) have begun to meet this challenge. This class of materials promises low-cost solution processing together with favorable intrinsic properties for optoelectronic applications, and have attracted a significant research effort after initial demonstrations of promising performances in photovoltaics,[1,2] light emitting diodes,[1,3] and lasing.[4–6] However, several challenges remain before improvements in performance, reproducibility, and reliability of devices under continuous operating conditions can be realized.[1] Addressing such matters inevitably requires a fundamental understanding of the intrinsic photophysical properties of bulk perovskites at operating conditions relevant for optoelectronic applications.

Currently, the details of charge carrier dynamics in organic-inorganic perovskites are still under debate. More precisely, there is a lack of understanding of the local intrinsic kinetics of photoexcited carriers in perovskite thin films, serving as active layers in solar cells, at device operating conditions. This knowledge requires replicating solar illumination excitation densities under broadband spectral excitation. To date, most investigations of light emission have been conducted at narrow spectral bandwidths, which may not capture the larger picture relevant for practical solar cell devices. Furthermore, due to sample inhomogeneities, local spatial interogation of optical properties is the best approach to relate structural characteristics to charge carrier dynamics. In

Dr. J.-C. Blancon, Dr. J. J. Crochet
Los Alamos National Laboratory
Physical Chemistry and Applied Spectroscopy
Los Alamos, NM 87545, USA
E-mail: jcrochet@lanl.gov
Dr. W. Nie, Dr. G. Gupta, Dr. A. D. Mohite
Los Alamos National Laboratory
Materials Synthesis and Integrated Devices
Los Alamos, NM 87545, USA
Dr. A. J. Neukirch, Dr. S. Tretiak
Los Alamos National Laboratory
Theoretical Chemistry and Molecular Physics
Los Alamos, NM 87545, USA
Dr. L. Cognet
Université de Bordeaux
Laboratoire Photonique Numérique et Nanosciences
UMR 5298, F-33400 Talence, France
Dr. L. Cognet
Institut d'Optique & CNRS
LP2N UMR 5298, F-33400 Talence, France

DOI: 10.1002/adfm.201505324

particular, for future improvements in device performance, it is important to decipher the dynamics of charge carriers in these materials at photoexcitation densities close to operating conditions at the microscale.

Despite several attempts to correlate the optical properties and photoexcited carrier dynamics within a given material morphology,[2,7–9] only a few reports have explored optical properties at the microscale or at the single grain size in thin films for practical applications.[2,9] Two of the major hindrances to such studies have been low crystalline quality and small grain sizes. On the other hand, there have been several attempts to investigate the optical properties and dynamics of carriers in bulk perovskite thin films, which consists of ensembles of grains. Typically this is performed at room temperature, using light emission[2,10–18] and absorption[11,14,19–23] characteristics to develop photophysical models. The first set of studies, hypothesizing a mixed response of excitonic and free-carrier photoexcitations, suggested extraordinary charge carrier diffusion lengths derived from nearly monoexponential photoluminescence (PL) decays.[10,11] Others have observed mixed monomolecular and bimolecular mechanisms which were attributed to the competition of trap assisted and free carrier recombination.[12,14,15,18,20] These results are in sharp contrast to what is expected in conventional bulk semiconducting direct band-gap materials with high crystallinity, which at room temperature should display a pure bimolecular recombination of free charges carriers.[24,25] Monomolecular decay of photoluminescence is only observed when electronic defects or excitonic effects dominate.

The growth of organic-inorganic perovskite crystals has recently reached a milestone with the synthesis of thin films with large crystalline grain structures by solution processing.[2] Moreover, these large grains have been reported to be free of deep level electronic impurities resulting in near intrinsic transport properties as well as stable and reliable solar cell performances. For these reasons, they offer a new opportunity to access the local intrinsic photophysical properties of these unique materials.

In this investigation, we unify the microscale dynamics of photoexcited carriers and macroscale solar cell performance of large grain methylammonium halide perovskite thin films. Most importantly, we demonstrate a pure bimolecular recombination through confocal time-resolved photoluminescence (TRPL) spectroscopy in large crystalline grains over a broad spectral range at excitation densities relevant for photovoltaic applications. This is a textbook signature of defect-free bulk direct band gap semiconducting materials, where the bimolecular recombination of photoexcited electrons and holes *via* radiative[24,25] and non-radiative[26] decay is the prevailing relaxation processes. By comparing bimolecular coefficients obtained using Langevin theory and derived from photoluminescence decays, we infer that freely recombining photoexcited carriers do not lead to major losses in photovoltaic devices because of efficient charge extraction. Additionally, measurements of an operating solar cell device under open circuit conditions (where carriers are not extracted from the cell) demonstrate that bimolecular recombination remains the sole decay channel of photoexcited charges and any defects formed during device fabrication are minor. These results demonstrate that solution cast large-area organic–inorganic perovskites have a technological potential in optoelectronics comparable to conventional semiconducting systems, and superb photovoltaic performance can be attributed to suppressed electron–hole recombination and negligible deep level electronic impurities.

2. Results and Discussion

2.1. Unambiguous Bimolecular Recombination in Large-Grain Perovskites

Thin films of crystalline grains of mixed halide perovskite $CH_3NH_3PbI_{3-x}Cl_x$ synthesized *via* a hot-casting method were used in this study.[2] The optical properties and carrier dynamics were investigated using microscale confocal spectroscopy and time-resolved PL (Note S1, Supporting Information). This microscale approach locally interrogated, with micrometer resolution (≈ 1 μm^2), the optical response of a single large-area grains (>100 μm in diameter) residing in an ≈ 300 nm thick perovskite thin film deposited on a glass substrate (**Figure 1**a, inset). The inner region of the large-area grain is relevant for photovoltaic applications as grain-boundaries in these large grains have a minor impact on the overall device performance, as demonstrated in our previous work.[2] Figure 1a shows the absolute absorption coefficient (α) and normalized photoluminescence spectrum measured confocally within a single large-area grain. The emission and absorption band-edge, observed at 1.626 ± 0.002 eV (763 nm) and 1.62 ± 0.01 eV (765 nm), respectively, display a relatively small Stokes shift at ambient conditions (Figure 1a). The absorption coefficient was obtained by correcting for multiple reflections occurring at the air/film and film/substrate interfaces and we deduced an $\alpha \approx 2.5 \times 10^4$ cm^{-1} at the band-edge in the near infrared that increases by an order of magnitude over the visible spectral range. From these results we also extracted the real and imaginary parts of refractive index (Figure S1 and Note S2, Supporting Information) demonstrating an acceptable agreement with our density functional theory (DFT) calculations (Figure S2 and Note S3, Supporting Information) and other recent studies.[21–23,27] We emphasize the importance of determining the absolute absorption coefficient for correctly interpreting the dynamics of carriers and the quantum efficiency of solar cell devices through accurate estimates of the carrier excitation density (Figure S1, Supporting Information). Accurate determinations of α also allow for comparing the photoexcited carrier density (N_0) achievable in our TRPL experiment to N_0 obtained in a planar solar cell under standard AM1.5 global illumination. With our TRPL system, featuring a wavelength-tunable 6-ps-pulsed-monochromatic laser excitation at 1 MHz, one solar irradiance (1 Sun) translates into a lower limit of $N_0 = 6.5 \times 10^{15}$ cm^{-3} and reaching values above 8×10^{15} cm^{-3} when considering the device geometry.

For quantitative analysis, time-resolved photoluminescence was performed on the same grain as the absorption and photoluminescence measurements using time-correlated single-photon counting (see details in Note S1, Supporting Information). Figure 1b shows the time-dependent photoluminescence intensity at the band-edge after excitation at 690 nm (1.80 eV) generating an equivalent excitation density of less than

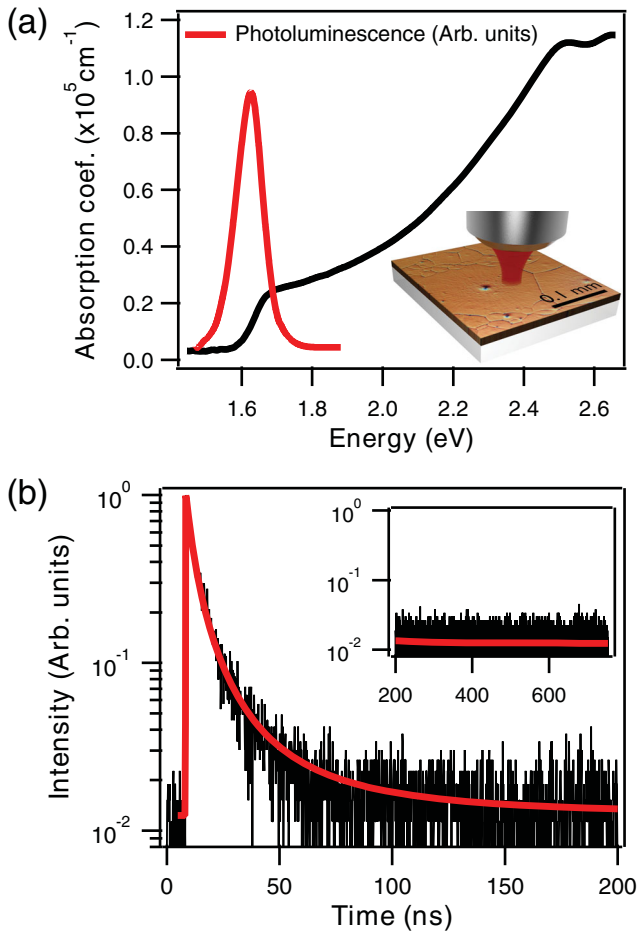

Figure 1. a) Absolute value of the absorption coefficient (black) and the PL spectrum (red). Inset: Phase contrast microscope image of a large-area grain organic-inorganic perovskite thin film deposited on glass. A schematic of how the confocal microscopy experiment probes a single grain is also shown. b) Time-correlated single photon counting histogram of the PL (black) and the bimolecular recombination model (red). Inset: Same showing the data at longer times.

4 Suns of irradiance ($N_0 = 2.8 \times 10^{16}$ cm^{-3}). The decay kinetics was modeled with a numerical solution to the first order rate equation describing the recombination of valence and conduction band states, coupled to a least squares optimization of the rate constant. Briefly, a focused laser pulse of photon energy, $\hbar\omega$, described by the charge density generation rate $G = \frac{P}{S\hbar\omega} A\alpha$ (where P is the laser power, S is the spot size, A is the thin film absorbance; see Note S2, Supporting Information), creates a nonequilibrium distribution of carriers in the valence and conduction bands (see also Figure 4). These carriers quickly relax to the band-edge on a picosecond-time scale,[11,20] which is unresolved in our experiments. Subsequently, the recombination of carriers is modeled by a pure band-to-band or bimolecular recombination, $\dot{N} = G - \gamma_b N^2$, of the nonequilibrium carrier density $N(t)$ (assuming equivalent photoexcited carrier density in the valence and conduction bands) described by a single bimolecular coefficient γ_b that includes both radiative and non-radiative processes.[24–26] Here the intensity of light emission is given as: $I_{PL} \propto N^2$, as will be demonstrated later. An example of the accuracy of this model is shown in Figure 1b where an excellent fit is displayed for the only free parameter $\gamma_b = 5.3 \times 10^{-9}$ cm^3 s^{-1}. Interestingly, this bimolecular recombination coefficient is order(s) of magnitude larger than previous reports on smaller-grain-structured organic-inorganic samples,[6,9,12,14,15,18,20] and comparable to that of typical direct-gap semiconductors.[28,29] Again, this result attests both the crystalline quality of our samples and that the photoexcitation of free charge carriers is the dominating kinetic process. However, γ_b is most likely influenced by photon recycling because of a small photoluminescence Stokes shift and a large absorption coefficient.[25,30,31] We therefore expect this value to be a lower bound of the recombination rate and further enhancements may be made in planar perovskite devices by limiting the angle of photon emission.[32,33] The determined recombination rate at this excitation energy (≈1.8 eV) corresponds to an approximate 7 ns effective electron–hole recombination lifetime, and this result unambiguously demonstrates that free carriers are the main photoexcitation in these materials. This is in agreement with recent reports of very small exciton binding energies (a few meV) at room temperature,[21,34] and possible ultra-fast exciton dissociation due to strong screening the electron–hole interaction by phonons and collective rotational motion of the organic cations (CH_3NH_3).[35,36]

2.2. Density Dependent Emission Intensity and Dynamics

Investigating the dependence of the recombination dynamics on the photoexcitation density is necessary to fully understand the relaxation processes of excess free charge carriers. In general, the photoluminescence intensity for electron–hole pair recombination is expressed as $I_{PL} \approx N_C N_V$ (where N_C is the conduction band density and N_V is the valence band density). Photoluminescence can also arise from recombination of an electron or hole with a charged shallow defect such that the charge densities should be re-defined as $N_C(t) = N(t) + N_u$ in the case of n-doping and $N_V(t) = N(t) + N_u$ in the case of p-doping. The equilibrium free carrier density N_u, encompassing n-type or p-type unintentional doping, is related to intrinsic defects. Theoretical investigations have associated this type unintentional doping to mainly Frenkel-type point defects, including vacancies, interstitials, and substitutions, and demonstrated that defects with small formation energies are all shallow trap states due the ionic nature of the material.[37,38] In particular, donors and acceptors act as both a source of doping and recombination centers (non-radiative) for excess carriers. A donor (acceptor) is a shallow level impurity which has an energy level just below (above) the conduction (valence) bands and can easily transfer an electron (hole) to the band, such that $D^0 \rightleftarrows D^+ + e^-$ ($A^0 \rightleftarrows A^+ + h^+$). On the other hand, deep level impurities are trap states and are composed of defects with large formation energies, however are much lower in density. Moreover, Schottky-type, neutral vacancy pair defects of PbI_2 and CH_3NH_3I are presumably abundant in solution-cast growth and are neutral de-localized states within the bands that do not contribute to doping. These defects are not expected to be major (non-radiative) recombination centers for carriers.[37] Our

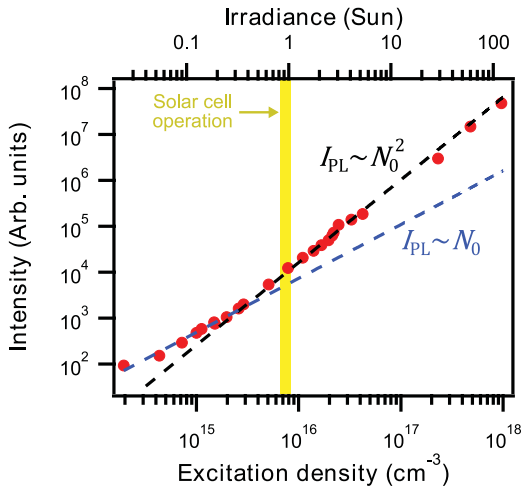

Figure 2. Photoluminescence intensity as a function of the photoexcitation density. Dashed lines are fit of the data.

preliminary measurements of field-effect transistor responses, which will be reported elsewhere, suggest a slight n-type doping in thin films grown by the method above. Thus, in the case of defects in the conduction band, the time-dependent photoluminescence intensity becomes $I_{PL}(t) \approx N^2 + NN_u$, and in the steady state limit $I_{PL} \approx N_0^2 + N_0N_u$. These two regimes of light emission in the steady state, free carrier and unpassivated defect assisted emission, were clearly identified by performing an excitation intensity dependent integrated photoluminescence study (**Figure 2**). This allowed for an estimate of an equilibrium density associated with unintentional doping due to intrinsic defects of $N_u \approx 2.5 \times 10^{15}$ cm^{-3}. This is equivalent to ≈ 0.3 Sun irradiance of photoexcitation. For an excitation density of $N_0 > N_u$, the regime in which solar cells operate, the photoluminescence intensity scales as $I_{PL} \approx N^2$ where excess free carriers mostly undergo bimolecular recombination after having passivated the equilibrium background charge.

Following steady state measurements, the dynamics of photoexcited carriers were investigated by TRPL over a relatively broad range of excitation densities at a photon energy of 1.8 eV (**Figure 3**). A general model of the carrier dynamics considering defect levels (trap states) probed by TRPL is given by the first-order rate equations

$$\dot{N} = G - \gamma_b N^2 - \gamma_\downarrow N + \gamma_\uparrow N_D$$

$$\dot{N}_D = \gamma_\downarrow N - \gamma_\uparrow N_D - \gamma_t N_D \quad (1)$$

where all quantities are defined in the schematics and captions of **Figure 4**. The time-dependent photoluminescence signal is given by $I_{PL} \approx xN^2 + (1-x)NN_u$, where x is either

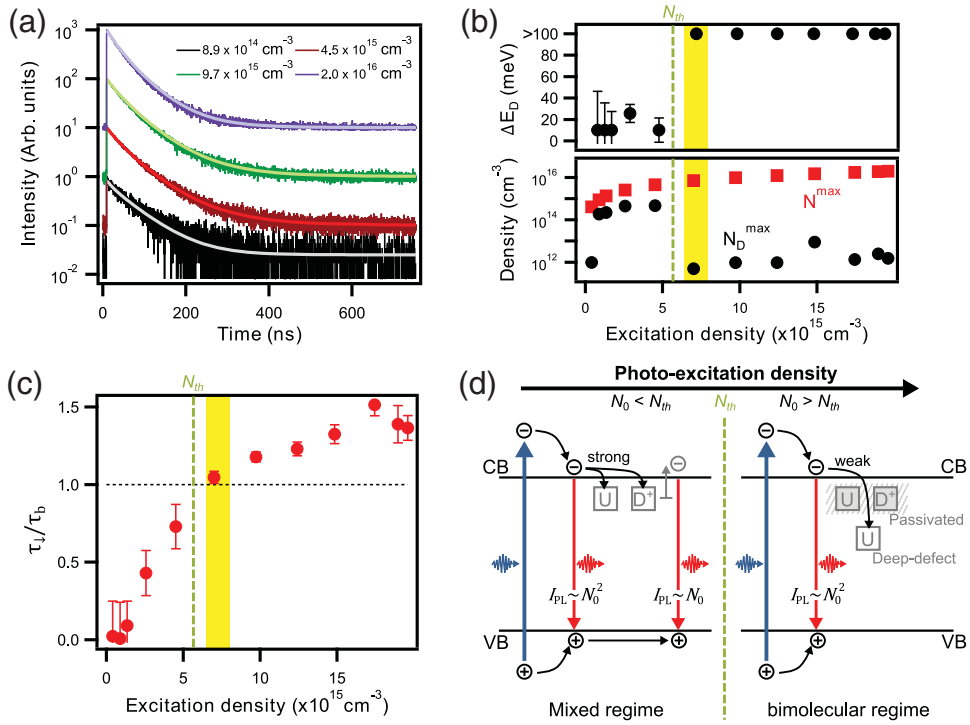

Figure 3. a) Time-correlated single photon counting histograms of the PL (dark colors) exciting at 690 nm (1.80 eV) and the recombination models (light colors) for different excitation densities. b) ΔE_D and maximum density of N, N_D, as well as c) lifetime ratios derived from the fitting of the data as a function of excitation density. The vertical dashed line at the saturation threshold excitation density N_{th} locates the transition between the mixed regime and the bimolecular regime. d) Schematic of the main photophysical processes in hybrid perovskites. In the mixed regime, after absorption of a photon, the main relaxation path is trap-assisted non-radiative recombination *via* a shallow charged (shown as a donor state D^+) or neutral (U) defect. The bimolecular recombination involves a photoexcited free hole, which recombines with either a photoexcited free electron or a bound electron to a donor state. In the bimolecular regime, shallow trap states have been passivated and the main relaxation process is the bimolecular recombination of photoexcited carriers.

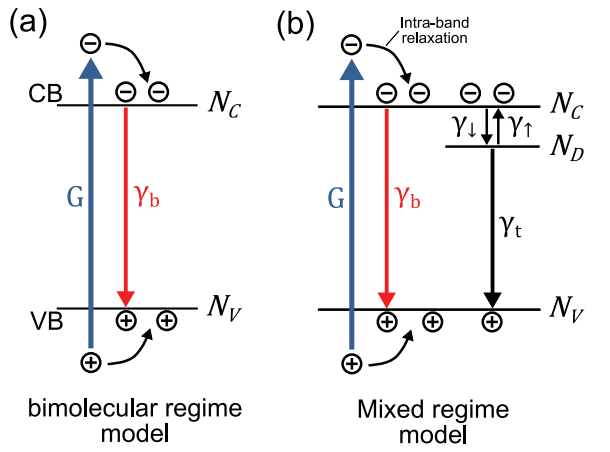

Figure 4. a) The dynamics of light emission is modeled by an excitation density generation rate provided by the laser *G* followed by an unresolved ultrafast relaxation to conduction and valence band edges (top and bottom arrows). The bimolecular recombination of conduction and valence band densities (N_C, N_V) is characterized by a single bimolecular coefficient γ_b. b) When defects are present, such as an electronic state characterized by a conduction band trap density N_D, a competing relaxation channel γ_t appears leading to kinetics that alter the bimolecular decay. Carriers can exchange density between the band-edge (N_C) and the trap state (N_D) *via* the rate couple ($\gamma_\downarrow$,$\gamma_\uparrow$) and the energy separation between N_C and N_D.

null for photoexcitation carrier density N_0 smaller than N_u or unity otherwise ($N_0 > N_u$), as discussed in the previous paragraph and Figure 2. After photogeneration (G), the excess of free carriers (N) at the band-edge can undergo bimolecular recombination ($\gamma_b N^2$) or exchange densities with trap states ($-\gamma_\downarrow N + \gamma_\uparrow N_D$) which relax by undergoing trap-assisted non-radiative recombination ($-\gamma_t N^D$), see the schematic in Figure 4. Here, we define the effective lifetime of free charge recombination $\tau_b = (\gamma_b N_0)^{-1}$ and characteristic lifetimes for the trap-assisted decay as $\tau_\downarrow = \gamma_\downarrow^{-1}$ and $\tau_t = \gamma_t^{-1}$. The exchange rates between the band-edge and trap states are directly related by the Boltzmann distribution defined by their energy splitting (ΔE_D): $\gamma_\uparrow = \gamma_\downarrow \exp\left(-\frac{\Delta E_D}{k_B T}\right)$, where k_B is the Boltzmann constant and T is the sample temperature (295 K). The TRPL kinetics were fit independently using a numerical solution to Equation (1) (see results in Figure S3, Supporting Information), yielding excellent fits with coefficients of determination R^2 exceeding 0.95, with the exception of the kinetics associated with $N_0 = 0.4 \times 10^{15}$ cm^{-3} for which $R^2 = 0.64$ due to a low signal-to-noise ratio at low photon detection yields in these experiments. For an excitation density of $N_0 < 5 \times 10^{15}$ cm^{-3}, the photoluminescence decays tend toward a more monoexponential response mixed with the bimolecular process of recombination in agreement with previous reports;[10,12,14] we label this as the "mixed regime." On the other hand, at higher excitation density, $N_0 > 5 \times 10^{15}$ cm^{-3}, the kinetics yield a pure bimolecular recombination behavior ("bimolecular regime"). Figure 3b,c displays the photoexcitation density dependence of the trap-state energy level (ΔE_D), the maximum occupation of both the band-edge (N^{max}) and trap state (N_D^{max}), and the ratio $\tau_\downarrow/\tau_b$ deduced from the global fitting procedure. Moreover, following the high quality fits with Equation (1), we hypothesize that Auger recombination is negligible in the range of excitation densities explored here, $N_0 < 10^{18}$ cm^{-3}, which is in agreement with the literature.[12,18]

All parameters directly related to the nature of the trap state N_D (ΔE_D, N_D^{max}, $\tau_\downarrow/\tau_b$) present a clear change in behavior at the threshold value $N_{th} \approx 5.5 \pm 1.0 \times 10^{15}$ cm^{-3}. This is identified as the photoexcitation density for which shallow trap states ($\Delta E_D < 25$ meV) are filled thus becoming transparent to carriers. The effective defect density in our large-area grains is somewhat lower than previous report in bulk perovskite materials[14,15] and comparable with a recent report on locally enhanced photoemission in microstructured or Cl-enriched materials.[9,39] Also, N_{th} is slightly larger than the unintentional doping density N_u measured in the static regime, which signifies that in the mixed regime photoemission arises from recombination of photoexcited carriers with charged shallow defects ($I_{PL} \approx N_0 N_u$). It also suggests that either non-doping neutral defects act as non-radiative recombination centers or n- and p-type intrinsic defect states partially compensate the static PL signal while TRPL only probes defects related to the minority carriers.[37,38] Concomitant to the switching of the trap-assisted decay path from shallow trap states ($\Delta E_D < 25$ meV) to deep trap states ($\Delta E_D > 100$ meV), we observe a strong reduction of the maximum occupation of the defect level N_D^{max} as well as an increase of the time constant ratio $\tau_\downarrow/\tau_b$ above unity. The latter implies that the excess carriers preferentially decay through the bimolecular recombination pathway for $\tau_\downarrow/\tau_b > 1$, where τ_b becomes the smallest effective lifetime. The former is explained by the lack of carrier exchange between the band-edge and trap states dictated by the Boltzmann distribution, where deep trap states should be unoccupied at room temperature (Figure S4, Supporting Information). From this we describe a physical picture where for $\Delta E_D < 25$ meV, a carrier occupying N_D decays non-radiatively at a rate γ_t but has also a chance to repopulate the band-edge with a rate $\gamma_\uparrow$, whereas, for $\Delta E_D > 100$ meV, a carrier has a negligible probability to transit from the trap-state to the band-edge ($\gamma_\uparrow \approx 0$) and $\gamma_\downarrow$ is the rate dominating the trap-assisted decay pathway (see also Figure S3c,d, Supporting Information). The intermediate situation where ΔE_D is comprised between 25 and 100 meV is not observed experimentally, however it is expected to show a more mild exchange of carriers between the trap state and the band-edge than in the case of shallow defects ($\Delta E_D < 25$ meV).

To summarize these results, schematically sown in Figure 3d, in the mixed regime ($N_0 < N_{th}$) the photoexcited carriers decay by undergoing both trap-assisted non-radiative recombination (dominant mechanism) and bimolecular recombination, whereas in the bimolecular regime ($N_0 > N_{th}$) the former decay pathway is either strongly damped (weak decay to deep trap states) or totally prohibited. The latter observation is in agreement with the low density of deep trap states in this material, since they require much higher energy to be formed.[37,38] From this low defect density we infer that large-area-grain structured solar cells operate in the bimolecular regime as reported in Figure 1b. This behavior is different than previous studies reporting solar cell operation in the mixed regime involving trap-assisted recombination and bimolecular recombination to doping induced dark carriers,[15,39] and the pure bimolecular regime only being reached at tens of solar irradiance.[15]

2.3. Photophysics over Broadband Light Excitation

In order to gain a more complete understanding of the photophysics in solar cells, we also examined the photoluminescence kinetics over a broad spectral range of excitation energies, between 1.8 and 2.7 eV (**Figure 5**a–c), while keeping the excess carrier density close to 1 Sun. First, the material was investigated in the bimolecular regime (Figure 5a, see also Figure 1b) and a pure bimolecular recombination process was observed with negligible trap-assisted decay (Figure 5c, black squares). The quality of the fits were characterized by $R^2 \geq 0.8$ and was mainly impaired by the inevitable noise in the data at such low photon flux densities (Figure S5, Supporting Information). The bimolecular coefficients were found to range from $\approx 5.3 \times 10^{-9}$ to less than 0.5×10^{-9} cm^3 s^{-1} (Figure 5b, see also Figure S5, Supporting Information). The error in the determination of these values is mainly related to the maximum 5% error on the absorption measurements. As shown in Figure 5b the bimolecular recombination coefficient depends strongly on the magnitude of the absorption coefficient and shows an anti-correlated behavior.

Next, we investigated the time-resolved photoluminescence response in the mixed regime and fit the data with Equation (1). In contrast to the bimolecular coefficient showing a strong spectral dependence, the trapping rate shows little spectral dependence (Figure 5c, blue circles), with a mean value of $\approx 4 \times 10^7$ s^{-1}. This suggests that the trap states probed over the whole spectral range of photoexcitation are of similar nature.

Finally, the static photoluminescence under monochromatic excitation was measured over a broad spectral range. Within a single large grain, a standard photoluminescence excitation map and integrated PL normalized to the absorption coefficient (equivalent to probing the relative change of the quantum yield) are displayed in Figure 5d. Fluctuations in intensity are in the maximum 5% error related to measurements of the absorption coefficient. The emission spectrum for each excitation energy was acquired by keeping the photoexcited density of carriers at $\approx$ 1 Sun of irradiance in order to reflect the conditions of illumination in photovoltaics. Over the entire range, no significant shift or broadening of the emission peak was observed, whereas a strong reduction of the PL intensity occurs toward the blue spectral region following a similar anti-correlated behavior in comparison to the absorption profile, as observed for the bimolecular coefficient.

The spectral profiles of the quantum yield and kinetic parameters are possibly explained by an increased amount of intraband scattering events of photoexcited carriers, with phonons and/or defect states, as they are photoexcited at energies further away from the band-edge (see schematics in **Figure 6**). This leads to an overall reduction of both the photoluminescence quantum yield and the bimolecular coefficient due to enhanced intraband non-radiative decay or decresed mobility taking place

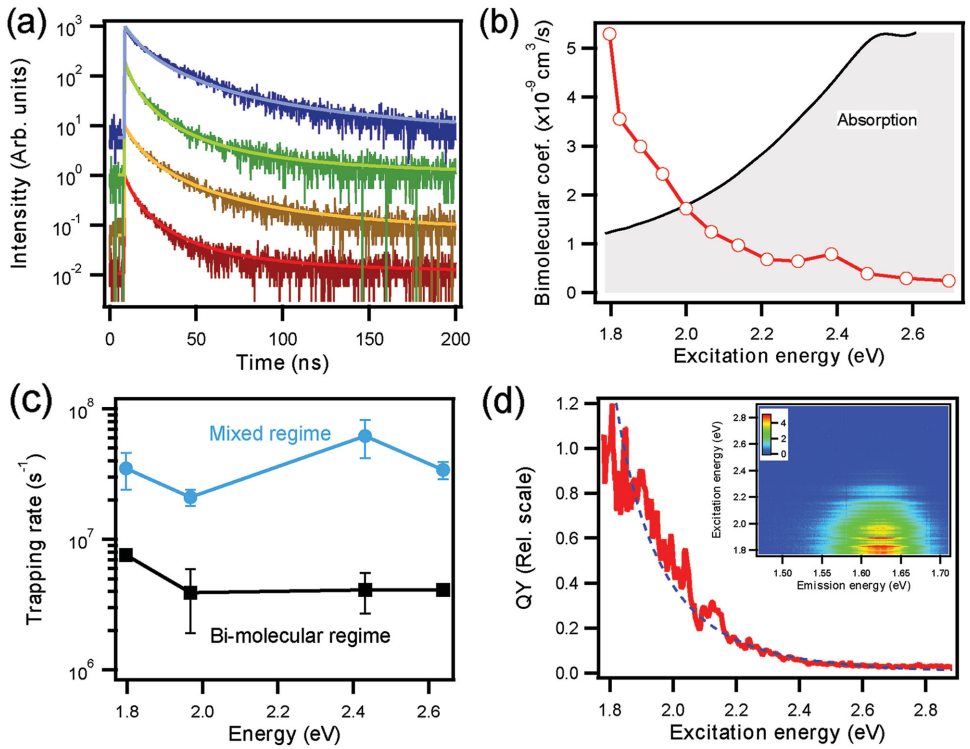

Figure 5. a) Time-correlated single photon counting histograms of the PL (dark colors) and the bimolecular recombination models (light colors) for selected excitation energies, from bottom to top: 1.88 eV (660 nm), 2.14 (580), 2.38 (520), and 2.58 (480). The photoexcitation density was kept in the bimolecular regime, *i.e.*, trap-assisted non-radiative recombination is negligible. b) Open symbols: Bimolecular coefficient γ_b derived from the fitting of the data, errors from the fits are negligible as compared to the symbol size however the maximum $\approx$ 5% error originating from the absorption measurements is not displayed. Gray region: Absorption coefficient profile. c) Trapping rate constants to shallow trap states (mixed regim, blue) and deep trap states (bimolecular regime, black). d) Excitation energy dependence of the relative quantum yield (red). Broken curve is the fit of the data with the model described in the main text. Inset: Color map of the photoluminescence quantum yield (rel. units) versus excitation (*y*-axis) and emission (*x*-axis) energy.

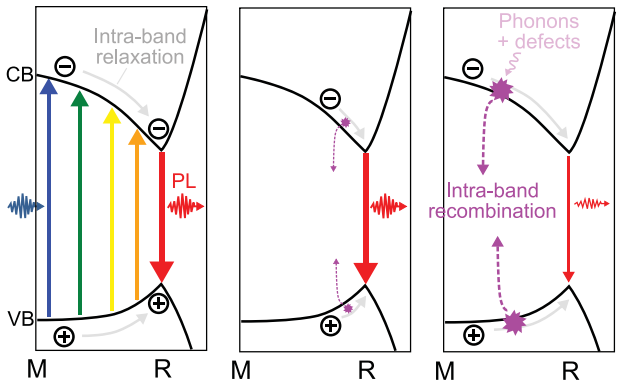

Figure 6. Schematics of the band structure of the high-temperature pseudocubic phase of perovskite. Adapted with permission.[41] Copyright, 2015 American Chemical Society) during: photoexcitation and photoemission (left), intraband relaxation for photoexcitation close to the bandgap energy (middle), and intraband relaxation for high-energy photoexcitation (right). Optical excitations generate free carriers in the valence ($E_{1/2,g}$) and conductions ($E_{1/2,u}$) bands which relax toward the R point where the emission takes place.

at higher energy during relaxation (Figure 6, middle and right panels). This hypothesis was drawn from: the similar nature of trap states across the visible spectrum, the broadband absorption mechanisms as described by Even et al.[35,40,41] (also sketched in Figure 6, left panel), and the reports of a phonon bottleneck and enhanced carrier-impurity scattering phenomena for higher energy photoexcitation.[42,43] Qualitatively, we describe the intraband relaxation in reciprocal space *via* the differential equation: $n(k) = -P_i n(k)$, with $n(k)$ being the carrier density at wave vector k and P_i the probability of carriers intraband recombination in k-space (assumed to be constant for simplicity). Using the band dispersion relation $E = \frac{\hbar k^2}{2m^*}$ along the R-M direction in k-space, where m^* is the effective mass,[44,45] the carrier density at the R-point following excitation at $E(k)$ is proportional to $\exp[-P_i\sqrt{2m^*E}/\hbar]$, which yields a reasonable qualitative fit to the integrated PL (Figure 5d, dashed line). From above spectral dependent TRPL results, we estimated an upper limit of the trap saturation threshold density N_{th} over a broad spectral range (Figure S6, Supporting Information), demonstrating that the passivation of shallow trap states is observed at values below 1 Sun of excitation density for photon energies below ≈ 2 eV and slightly higher than 1 Sun above 2 eV. This observation also corroborates the higher probability for carriers generated with blue-light excitation to undergo trap-assisted recombination as they are exposed to a higher density of trap states, both shallow and deep. In addition to this effect, we can expect surface trap states, self-trapped charges or self-trapped excitons, originating from electron–phonon coupling at the thin film surface,[46] to be prevalent under blue-light excitation which probes a shallow layer of the thin film (see also Figure S7, Supporting Information).

2.4. Solar Cell Performance

To confirm that trap-assisted recombination is not an influential process in a high quality-operating device, we investi-

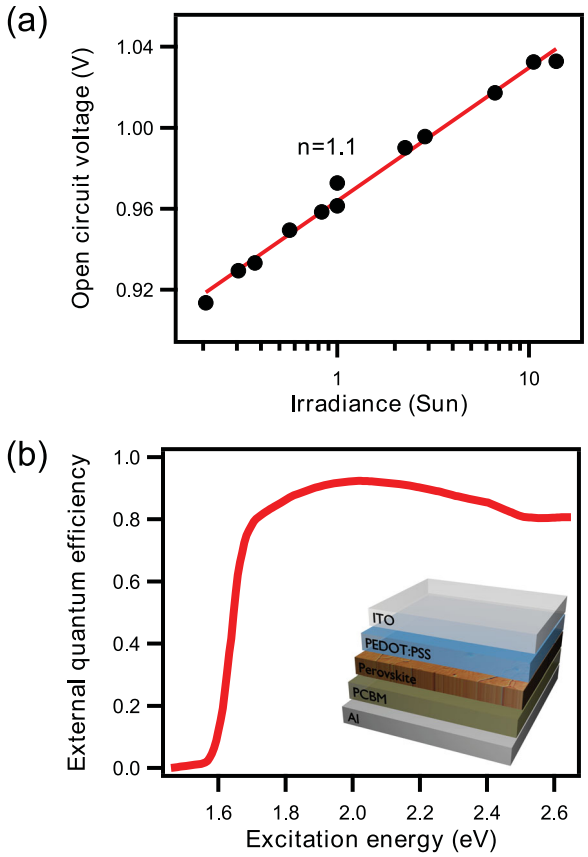

Figure 7. a) Open circuit voltage as a function of irradiance (filled black circles). The line is a fit showing an ideality factor close to 1 suggesting a dominating bimolecular recombination of photoexcited carriers. b) Spectrally resolved absolute value of the external quantum efficiency measured on a full device. The inset is a schematic of the device geometry.

gated the performance of a planar solar cell (see the inset in **Figure 7**b) with the same material active region as above over a wide range of illumination irradiance. This was done by measuring V_{OC} as a function of light intensity (Figure 7a). The cell was illuminated with the standard AM 1.5 solar spectrum with irradiance ranging from 0.2 to 14 Sun, in a regime where Auger recombination effects are expected to be negligible (the onset of Auger effects have been reported for carrier densities created by ≈100 Sun).[12,18] In this measurement, all of the carriers recombine in the active layer because there is no net current flow. Here the slope of V_{OC} versus irradiance on a linear-log scale determines the so-called ideality factor n. More precisely, nk_BT/q is the slope of the linear curve where q is the elementary charge. When $n = 1$ the measurement suggests that bimolecular recombination is the dominating decay mechanism in the active layer.[47] Larger values up to $n = 2$ indicate trap-assisted recombination is prevalent and the material has a relatively large density of deep level electronic impurities that mask bimolecular recombination. For this device and material we found $n \approx 1.1$ where the small deviation from an ideality of 1 is expected to result from the presence of a few grain boundaries under the contact and illumination area.[2] This confirms that bimolecular recombination is the dominating dynamics for carriers in this material at macroscopic scale and that the scattering of carriers into deep

electronic defects does not alter the overall transport properties of devices. Moreover, both the micro- and macroscale carrier dynamics results are reflected in the external quantum efficiency under 1 Sun illumination that yields values larger than 80% above the band-gap (Figure 7b). This clearly suggests few losses after absorption and nearly an 100% internal quantum efficiency for large grains, in agreement with recent studies.[21,48,49]

2.5. Microscopic Origins of Photovoltaic Efficiency

Knowledge of the underlying physics of shallow trap passivation, bimolecular recombination, and spectral variations of the photoluminescence kinetics and intensity are important for understanding the transport properties of large grain perovskites. Using Langevin theory describing the recombination of free carriers in diffusion limited semiconductors, the spectral and excitation density dependence of the effective diffusion constant of carriers can be derived as $D = \frac{\gamma_b}{4\pi r_C}$ (Figure S5, Supporting Information), using the Onsager radius $r_c = \frac{k_c q^2}{\varepsilon_s k_B T}$, where k_C is the Coulomb constant, ε_0 is the vacuum permittivity, and $\varepsilon_S = 35$ is the static dielectric constant[50] (see details in Note S4, Supporting Information). Here, values of D are in the range $\approx 0.1–2.5 \times 10^{-3}$ cm^2 s^{-1} depending on excitation energy, with similar spectral dependences as γ_b. From the values of diffusion constant, at room temperature, we expect minority carrier mobilities in the range of $\approx 10^{-1} - 10^{-2}$ cm^2 V^{-1} s^{-1}, with a similar spectral profile as the diffusion constant and γ_b. These values are of the same magnitude as those reported for bulk $NH_3CH_3PbI_3$ (see refs.[51,52] and literature therein), however much smaller than what is expected theoretically.[51,53] Using derived mobilities from the bi-molecular coefficients, the Nernst–Townsend–Einstein relation would yield un-physical sub-fs elastic scattering mean free times, assuming effective masses reported in the literature.[44,45] Thus, we infer in these systems there must be an effective mass enhancement due to electron–phonon coupling linked to polaronic states[54–56] or carrier localization effects,[36] mostly likely caused by an orientational disorder of organic cation. In fact, it is understood that the orientational disorder of the organic cation (methylammonium ions) in the lattice is altered by polarized light, which can give rise to local structural distortions that cause changes in the electronic and vibrational landscape.[54,57–61] This may be reflected in the recent observations of giant photoinduced dielectric constants[62] and Glass coefficients[57] that increase linearly with broadband excitation intensity.

Further, lower-limit values of mobility predicted from first principle (140 cm^2 V^{-1} s^{-1} for holes and 466 cm^2 V^{-1} s^{-1} for electrons)[51] yield a Langevin bimolecular coefficient[63] of $\gamma_L = 3.1 \times 10^{-5}$ cm^3 s^{-1}. This provides a lower limit for the transport Figure of merit which reflects a suppression of electron–hole recombination, $\frac{\gamma_b}{\gamma_L} \approx 1.7 \times 10^{-4}$. Using typical mobilities in our solar cells,[2,64] ≈ 5 cm^2 V^{-1} s^{-1} or more for 15% power conversion efficiency, we find $\gamma_L = 5.2 \times 10^{-7}$ cm^3 s^{-1} and $\frac{\gamma_b}{\gamma_L} < 1 \times 10^{-2}$. This implies that perovskite solar cells fabricated in this fashion operate in the non-Langevin recombination regime, which is necessary for efficient photovoltaic devices with low charge carrier mobilities in order to prevent significant losses due to recombination competing with the charge extraction processes.[63] In other words, the lifetime of the charge carriers must be longer than their transit time in the intrinsic electric field in order to obtain efficient energy conversion in solar cells. This can be reformulated in terms of a mobility lower limit as $\mu > \frac{n_0 \gamma_b d^2}{V_{bi}}$, where V_{bi} is the built-in electric field potential (V_{bi} = 0.78 V in our solar cells)[64] with thickness d = 450 nm. We estimate $\mu > 10^{-2}$ cm^2 V^{-1} s^{-1} is necessary for efficient energy conversion. These conditions are in good agreement with our TRPL analysis, and fulfilled in our large-area grain perovskite material. This rational further explains the high performances observed in perovskite-based solar cells beyond having low deep level defect densities.

3. Conclusions

Our findings of pure bimolecular recombination are in stark contrast with previous reports on bulk organic-inorganic perovskite materials showing nearly exponential monomolecular processes at equivalent carrier densities or a combination of both bimolecular recombination and trap-assisted relaxation.[10,12,14,15,39,65] The origin of this discrepancy may result from small grains where crystal boundaries and defects result in dynamics that deviate from bimolecular recombination because of monomolecular trap assisted recombination[2] (Figure 4b and Figure S8, Supporting Information). Notably, the observation of a pure bimolecular decay is unique for semiconducting solution-processed materials at this excitation density as trap-assisted and exciton recombination (both monomolecular kinetics) are usually dominating processes. Most importantly, our findings bridge the gap between the microscale optical properties and macroscale solar cell performance of crystalline methylammonium halide thin films. These results clearly demonstrate that devices based on solution processed thin film semiconductors can be operated in regimes free of impurities that degrade transport and alter optical properties. More broadly this work asserts the rapid progress in organic–inorganic perovskite based optoelectronics where experimentally determined intrinsic properties represent a clear departure from macroscopic ensembles of nanoparticle systems that are plagued by inhomogeneity and defects. Nevertheless, the mobility of charge carriers in perovskites remains significantly lower than conventional semiconductors, reflecting transport may be similar to that in organic systems without large deep level defect densities associated with multiple interfaces. Further understanding of the details of charge carrier localization and mobilities associated with the dynamic perovskite lattice[66] will aid in providing a physical picture of transport in these hybrid systems and pave the way for improved stability and performance in optoelectronic devices.

Supporting Information

Supporting Information is available from the Wiley Online Library or from the author.

Acknowledgements

This work was supported the Los Alamos National Laboratory LDRD program. L.C. acknowledges additional support from "INCa-Canceropole GSO." The authors also acknowledge the LANL Institutional Computing (IC) Program for providing computational resources. The authors declare no competing financial interests.

Received: December 10, 2015
Revised: January 29, 2016
Published online: April 27, 2016

[1] S. D. Stranks, H. J. Snaith, *Nat. Nanotechnol.* **2015**, *10*, 391.
[2] W. Nie, H. Tsai, R. Asadpour, J.-C. Blancon, A. J. Neukirch, G. Gupta, J. J. Crochet, M. Chhowalla, S. Tretiak, M. A. Alam, H.-L. Wang, A. D. Mohite, *Science* **2015**, *347*, 522.
[3] Z.-K. Tan, R. S. Moghaddam, M. L. Lai, P. Docampo, R. Higler, F. Deschler, M. Price, A. Sadhanala, L. M. Pazos, D. Credgington, F. Hanusch, T. Bein, H. J. Snaith, R. H. Friend, *Nat. Nanotechnol.* **2014**, *9*, 687.
[4] G. Xing, N. Mathews, S. S. Lim, N. Yantara, X. Liu, D. Sabba, M. Grätzel, S. Mhaisalkar, T. C. Sum, *Nat. Mater.* **2014**, *13*, 476.
[5] H. Zhu, Y. Fu, F. Meng, X. Wu, Z. Gong, Q. Ding, M. V. Gustafsson, M. T. Trinh, S. Jin, X.-Y. Zhu, *Nat. Mater.* **2015**, *14*, 636.
[6] F. Deschler, M. Price, S. Pathak, L. E. Klintberg, D.-D. Jarausch, R. Higler, S. Hüttner, T. Leijtens, S. D. Stranks, H. J. Snaith, M. Atatüre, R. T. Phillips, R. H. Friend, *J. Phys. Chem. Lett.* **2014**, *5*, 1421.
[7] M. D. Bastiani, V. D'Innocenzo, S. D. Stranks, H. J. Snaith, A. Petrozza, *APL Mater.* **2014**, *2*, 081509.
[8] V. D'Innocenzo, A. R. Srimath Kandada, M. De Bastiani, M. Gandini, A. Petrozza, *J. Am. Chem. Soc.* **2014**, *136*, 17730.
[9] D. W. deQuilettes, S. M. Vorpahl, S. D. Stranks, H. Nagaoka, G. E. Eperon, M. E. Ziffer, H. J. Snaith, D. S. Ginger, *Science* **2015**, *348*, 683.
[10] S. D. Stranks, G. E. Eperon, G. Grancini, C. Menelaou, M. J. P. Alcocer, T. Leijtens, L. M. Herz, A. Petrozza, H. J. Snaith, *Science* **2013**, *342*, 341.
[11] G. Xing, N. Mathews, S. Sun, S. S. Lim, Y. M. Lam, M. Grätzel, S. Mhaisalkar, T. C. Sum, *Science* **2013**, *342*, 344.
[12] C. Wehrenfennig, G. E. Eperon, M. B. Johnston, H. J. Snaith, L. M. Herz, *Adv. Mater.* **2014**, *26*, 1584.
[13] C. Wehrenfennig, M. Liu, H. J. Snaith, M. B. Johnston, L. M. Herz, *J. Phys. Chem. Lett.* **2014**, *5*, 1300.
[14] Y. Yamada, T. Nakamura, M. Endo, A. Wakamiya, Y. Kanemitsu, *J. Am. Chem. Soc.* **2014**, *136*, 11610.
[15] S. D. Stranks, V. M. Burlakov, T. Leijtens, J. M. Ball, A. Goriely, H. J. Snaith, *Phys. Rev. Appl.* **2014**, *2*, 034007.
[16] T. C. Sum, N. Mathews, *Energy Environ. Sci.* **2014**, *7*, 2518.
[17] J. A. Christians, J. S. Manser, P. V. Kamat, *J. Phys. Chem. Lett.* **2015**, *6*, 2086.
[18] M. Saba, M. Cadelano, D. Marongiu, F. Chen, V. Sarritzu, N. Sestu, C. Figus, M. Aresti, R. Piras, A. Geddo Lehmann, C. Cannas, A. Musinu, F. Quochi, A. Mura, G. Bongiovanni, *Nat. Commun.* **2014**, *5*, 5049.
[19] A. Marchioro, J. Teuscher, D. Friedrich, M. Kunst, R. van de Krol, T. Moehl, M. Grätzel, J.-E. Moser, *Nat. Photonics* **2014**, *8*, 250.
[20] J. S. Manser, P. V. Kamat, *Nat. Photonics* **2014**, *8*, 737.
[21] Q. Lin, A. Armin, R. C. R. Nagiri, P. L. Burn, P. Meredith, *Nat. Photonics* **2015**, *9*, 106.
[22] M. Anaya, G. Lozano, M. E. Calvo, W. Zhang, M. B. Johnston, H. J. Snaith, H. Míguez, *J. Phys. Chem. Lett.* **2014**, *6*, 48.
[23] P. Löper, M. Stuckelberger, B. Niesen, J. Werner, M. Filipič, S.-J. Moon, J.-H. Yum, M. Topič, S. De Wolf, C. Ballif, *J. Phys. Chem. Lett.* **2015**, *6*, 66.
[24] G. Lasher, F. Stern, *Phys. Rev.* **1964**, *133*, A553.
[25] E. Yablonovitch, *Phys. Rev. Lett.* **1987**, *58*, 2059.
[26] J. Liu, O. V. Prezhdo, *J. Phys. Chem. Lett.* **2015**, *6*, 4463.
[27] Y. Jiang, M. A. Green, R. Sheng, A. Ho-Baillie, *Sol. Energy Mater. Sol. Cells* **2015**, *137*, 253.
[28] A. Dmitriev, A. Oruzheinikov, *J. Appl. Phys.* **1999**, *86*, 3241.
[29] Y. P. Varshni, *Phys. Status Solidi B* **1967**, *19*, 459.
[30] P. Asbeck, *J. Appl. Phys.* **1977**, *48*, 820.
[31] Y. Yamada, T. Yamada, L. Q. Phuong, N. Maruyama, H. Nishimura, A. Wakamiya, Y. Murata, Y. Kanemitsu, *J. Am. Chem. Soc.* **2015**, *137*, 10456.
[32] E. D. Kosten, B. M. Kayes, H. A. Atwater, *Energy Environ. Sci.* **2014**, *7*, 1907.
[33] W. E. I. Sha, X. Ren, L. Chen, W. C. H. Choy, *Appl. Phys. Lett.* **2015**, *106*, 221104.
[34] A. Miyata, A. Mitioglu, P. Plochocka, O. Portugall, J. T.-W. Wang, S. D. Stranks, H. J. Snaith, R. J. Nicholas, *Nat. Phys.* **2015**, *11*, 582.
[35] J. Even, L. Pedesseau, C. Katan, *J. Phys. Chem. C* **2014**, *118*, 11566.
[36] J. Ma, L.-W. Wang, *Nano Lett.* **2015**, *15*, 248.
[37] J. Kim, S.-H. Lee, J. H. Lee, K.-H. Hong, *J. Phys. Chem. Lett.* **2014**, *5*, 1312.
[38] W.-J. Yin, T. Shi, Y. Yan, *Appl. Phys. Lett.* **2014**, *104*, 063903.
[39] E. M. Hutter, G. E. Eperon, S. D. Stranks, T. J. Savenije, *J. Phys. Chem. Lett.* **2015**, *6*, 3082.
[40] J. Even, *J. Phys. Chem. Lett.* **2015**, *6*, 2238.
[41] J. Even, L. Pedesseau, C. Katan, M. Kepenekian, J.-S. Lauret, D. Sapori, E. Deleporte, *J. Phys. Chem. C* **2015**, *119*, 10161.
[42] M. B. Price, J. Butkus, T. C. Jellicoe, A. Sadhanala, A. Briane, J. E. Halpert, K. Broch, J. M. Hodgkiss, R. H. Friend, F. Deschler, *Nat. Commun.* **2015**, *6*, 8420.
[43] M.-H. Du, *J. Phys. Chem. Lett.* **2015**, *6*, 1461.
[44] P. Umari, E. Mosconi, F. De Angelis, *Sci. Rep.* **2014**, *4*, 4467.
[45] M. R. Filip, C. Verdi, F. Giustino, *J. Phys. Chem. C* **2015**, *119*, 25209.
[46] X. Wu, M. T. Trinh, D. Niesner, H. Zhu, Z. Norman, J. S. Owen, O. Yaffe, B. J. Kudisch, X.-Y. Zhu, *J. Am. Chem. Soc.* **2015**, *137*, 2089.
[47] L. J. A. Koster, V. D. Mihailetchi, R. Ramaker, P. W. M. Blom, *Appl. Phys. Lett.* **2005**, *86*, 123509.
[48] J. M. Ball, S. D. Stranks, M. T. Hörantner, S. Hüttner, W. Zhang, E. J. W. Crossland, I. Ramirez, M. Riede, M. B. Johnston, R. H. Friend, H. J. Snaith, *Energy Environ. Sci.* **2015**, *8*, 602.
[49] B. Yang, O. Dyck, J. Poplawsky, J. Keum, A. Puretzky, S. Das, I. Ivanov, C. Rouleau, G. Duscher, D. Geohegan, K. Xiao, *J. Am. Chem. Soc.* **2015**, *137*, 9210.
[50] N. Onoda-Yamamuro, T. Matsuo, H. Suga, *J. Phys. Chem. Solids* **1992**, *53*, 935.
[51] X. Y. Chin, D. Cortecchia, J. Yin, A. Bruno, C. Soci, *Nat. Commun.* **2015**, *6*, 7383.
[52] F. Li, C. Ma, H. Wang, W. Hu, W. Yu, A. D. Sheikh, T. Wu, *Nat. Commun.* **2015**, *6*, 8238.
[53] Y. He, G. Galli, *Chem. Mater.* **2014**, *26*, 5394.
[54] J. M. Frost, K. T. Butler, A. Walsh, *APL Mater.* **2014**, *2*, 081506.
[55] X.-Y. Zhu, V. Podzorov, *J. Phys. Chem. Lett.* **2015**, *6*, 4758.
[56] T. M. Brenner, D. A. Egger, A. M. Rappe, L. Kronik, G. Hodes, D. Cahen, *J. Phys. Chem. Lett.* **2015**, *6*, 4754.
[57] H. T. Fan Zheng, *J. Phys. Chem. Lett.* **2014**, *6*, 31.
[58] C. Motta, F. El-Mellouhi, S. Kais, N. Tabet, F. Alharbi, S. Sanvito, *Nat. Commun.* **2015**, *6*, 7026.

[59] A. M. A. Leguy, J. M. Frost, A. P. McMahon, V. G. Sakai, W. Kockelmann, C. Law, X. Li, F. Foglia, A. Walsh, B. C. O'Regan, J. Nelson, J. T. Cabral, P. R. F. Barnes, *Nat. Commun.* **2015**, *6*, 7241.
[60] A. A. Bakulin, A. Rao, V. G. Pavelyev, P. H. M. van Loosdrecht, M. S. Pshenichnikov, D. Niedzialek, J. Cornil, D. Beljonne, R. H. Friend, *Science* **2012**, *335*, 1340.
[61] H. Tsai, W. Nie, P. Cheruku, N. H. Mack, P. Xu, G. Gupta, A. D. Mohite, H.-L. Wang, *Chem. Mater.* **2015**, *27*, 5570.
[62] R. S. S. Emilio, J. Juarez-Perez, *J. Phys. Chem. Lett.* **2014**, *5*, 2390.
[63] A. Pivrikas, G. Juška, A. J. Mozer, M. Scharber, K. Arlauskas, N. S. Sariciftci, H. Stubb, R. Österbacka, *Phys. Rev. Lett.* **2005**, *94*, 176806.
[64] X. Sun, R. Asadpour, W. Nie, A. D. Mohite, M. A. Alam, *IEEE J. Photovolt.* **2015**, *5*, 1389.
[65] G.-J. A. H. Wetzelaer, M. Scheepers, A. M. Sempere, C. Momblona, J. Avila, H. J. Bolink, *Adv. Mater.* **2015**, *27*, 1837.
[66] J. M. Frost, K. T. Butler, F. Brivio, C. H. Hendon, M. van Schilfgaarde, A. Walsh, *Nano Lett.* **2014**, *14*, 2584.